Electrical resistivity of the heavy-fermion-filled cage compound $Ce_3M_4Sn_{13}$(M = Co, Rh, Ru) under high pressure

A. Ślebarski,[1,2] J. Goraus,[1] and P. Witas[1]
[1]*Institute of Physics, University of Silesia, Uniwersytecka 4, 40-007 Katowice, Poland*
[2]*Centre for Advanced Materials and Smart Structures, Polish Academy of Sciences, Okólna 2, 50-950 Wrocław, Poland*
(Received 8 May 2015; published 21 October 2015)

The effect of pressure on electrical resistivity of heavy-fermion compounds $Ce_3M_4Sn_{13}$, where M = Co, Rh, Ru, and the $La_3M_4Sn_{13}$ counterparts is studied in the framework of the fully relativistic full potential local orbital method. The experiment shows that the electrical resistivity of $Ce_3Co_4Sn_{13}$ and $Ce_3Rh_4Sn_{13}$ increases with pressure, a similar pressure effect is obtained for isostructural La-based reference metals, while opposite behaviors under pressure are documented for $Ce_3Ru_4Sn_{13}$ and $La_3Ru_4Sn_{13}$. The contrasting pressure dependent effects of $Ce_3Co_4Sn_{13}$ and $Ce_3Ru_4Sn_{13}$ are discussed. In order to clarify the various phenomena the band-structure calculations under applied pressure were performed. Here, we show that the resistivity increase with pressure arises from the formation of interband distances at the Fermi level in $Ce_3Co_4Sn_{13}$, this pseudo-gap-like effect is also pressure dependent, while in $Ce_3Ru_4Sn_{13}$ the opposite change of resistivity results from the suppression of spin fluctuations under pressure.

DOI: 10.1103/PhysRevB.92.155136 PACS number(s): 71.27.+a, 72.15.Qm, 71.20.−b

I. INTRODUCTION

Heavy-fermion (HF) Kondo lattices display various behaviors, still not well understood, which determine fundamental issues of experimental and theoretical investigations. Current research focuses on the physical properties associated with the possible quantum phase transitions between magnetic and *nonmagnetic* ground states in these materials, since the transition can be relatively easily attained by tuning the competing Ruderman-Kittel-Kasuya-Yosida (RKKY) and Kondo interactions. Several studies under external pressure on cerium-based systems have shown novel phenomena accompanying the presence of the quantum critical point (QCP), which show deviations from Landau Fermi-liquid theory in the electrical resistivity ρ, magnetic susceptibility χ, and specific heat C. The Doniach diagram [1] qualitatively explains the ground-state properties of a Kondo lattice system. The model is based on the relative strength of two competing phenomena, both dependent on the coupling J_{fs} between the local $4f$ moments and the conduction band: the RKKY magnetic interaction leading to the magnetic ground state below $T_{\rm RKKY} \sim J_{fs}^2 N(\epsilon_F)$ and Kondo effect depicted by $T_K \sim \exp[-1/J_{fs}N(\epsilon_F)]$, where $N(\epsilon_F)$ represents the density of states (DOS) at the Fermi energy. In localized f electron systems and in the systems with broad, flat, and degenerate bands $N(\epsilon_F)$ is generally expected to decrease with pressure [2]. However, in correlated electron Ce-based systems, the sharp peak in DOS due to $4f$ electron resonance is situated in close proximity to the Fermi energy. Dynamics of this resonance with respect to the Fermi energy can be profoundly different depending on whether the $4f$ apex is below or above the Fermi energy. Thus, one can expect that either a decrease or an increase in the density of states could be assigned to the general pressure effect. Therefore the increase of ρ with pressure in a typical heavy-fermion Kondo lattice system, when observed above Kondo temperature [3] or temperature of the coherence between Kondo ions in the lattice [2,4–6], is ascribed to the increase of J_{fs} with pressure [7,8]. A positive $\frac{d\rho}{dP}$ behavior has been recently observed for $Ce_3Co_4Sn_{13}$ [9]. Recent studies have shown that $Ce_3Co_4Sn_{13}$ exhibits a behavior characteristic of Kondo lattice systems with comparable Kondo and magnetic energy scales and is indeed near a QCP [10,11]; moreover, $C(T)/T$, $\chi(T)$, and $\rho(T)$ indicate below $T \sim 1$ K a presence of the antiferromagnetic correlations. We also demonstrated for $Ce_3Co_4Sn_{13}$ the positive pressure effect $\frac{d\rho}{dP}$ [12], much stronger for $T < T_D \approx 160$ K, i.e., below the subtle structural distortion at T_D, than the $\frac{d\rho}{dP}$ value obtained at the temperatures $T > T_D$. The positive value of $\frac{d\rho}{dP}$ was at $T < T_D$ also proved for $Ce_3Rh_4Sn_{13}$ [12], while for $Ce_3Ru_4Sn_{13}$ and its La counterpart $\frac{d\rho}{dP} < 0$. There are many experimental reports that show a decrease in the resistivity with pressure, i.e., $\frac{d\rho}{dP} < 0$, for La-based as well as other normal metals, which can be simply explained by a change in the chemical potential under pressure. This is, however, not a case of $La_3Ru_4Sn_{13}$; our band-structure calculations clearly documented that a maximum in DOS located exactly at the Fermi level does not have any dependence on the pressure within the pressure range $P \leqslant 2.6$ GPa. The main goal of this work is to understand why the value of $\frac{d\rho}{dT}$ in the system of isostructural $Ce_3M_4Sn_{13}$ compounds is negative for $Ce_3Ru_4Sn_{13}$ and $La_3Ru_4Sn_{13}$. We discuss these various pressure dependencies of the electrical resistivity as a result of overlapping of several effects, the most important being change of J_{fs} coupling and/or DOS at ϵ_F with pressure and different covalent bondings in the system of $Ce_3M_4Sn_{13}$ compounds. The recent investigations [13–15] revealed distinct anomalies in the electrical resistivity in the series of $Ce_3M_4Sn_{13}$ compounds at $T_D \sim 160$ K, as a result of a local structural deformation of the $(Sn2)_{12}$ cages. We explained [15] that this structural distortion significantly changes both the charge distribution inside the $(Sn2)_{12}$ cages and the charge density accumulation between Rh or Ru and Sn2 atoms, respectively, in $Ce_3Rh_4Sn_{13}$ [16] and $Ce_3Ru_4Sn_{13}$ [17]. Here, we present similar calculations for $Ce_3Co_4Sn_{13}$. The energy bands and the densities of states were calculated for respective $Ce_3M_4Sn_{13}$ compounds using the fully relativistic full potential local orbital method. The chemical bondings between different atoms were analyzed

based on the charge density maps obtained from band-structure calculations.

II. EXPERIMENTAL DETAILS

Polycrystalline $Ce_3M_4Sn_{13}$ and $La_3M_4Sn_{13}$ samples were prepared by arc melting the constituent elements on a water cooled copper hearth in a high-purity argon atmosphere with an Al getter, and then annealed at 870 °C for two weeks. All samples were carefully examined by x-ray-diffraction analysis and found to have a cubic structure (space group $Pm\bar{3}n$) [18]. As shown in Fig. 1, the unit cell contains two formulas of $Ce_3M_4Sn_{13}$ with Sn1, Ce, metal M, and Sn2 occupying the $2a$, $6d$, $8e$, and $24k$ Wyckoff sites, respectively (in the figure M = Co). Stoichiometry and homogeneity verified by the microprobe technique (scanning microscope JSM-5410) and by XPS analysis are close to the nominal ratio 3:4:13.

Ambient pressure electrical resistivity ρ was investigated by a conventional four-point ac technique using a Quantum Design physical properties measurement system. Electrical resistivity measurements under pressure were performed in a beryllium-copper, piston-cylinder clamped cell (for details, see Ref. [12]).

The band-structure calculations were accomplished using fully relativistic full potential local orbital method (FPLO9-00-34 computer code [19]) within the local spin density approximation (LSDA). The exchange correlation potential V_{xc} was used in the form proposed by Perdew and Wang [20]. The number of k points in the irreducible wedge of Brillouin zone was 20 for each component of the series; due to a large volume of the unit cell this number was found sufficient to obtain well-converged results. The spin-orbit interactions considered within fully relativistic calculations reduce symmetry of the magnetic unit cell depending on the chosen magnetization axis. In our calculations we used (0,0,1) as the chosen direction of the magnetization axis. Charge density was evaluated on a $52 \times 52 \times 52$ point grid within the unit cell. The calculations have been performed in a full relativistic spin-resolved way as the nonmagnetic calculations are inherently not reliable for heavy elements such as rare-earth based compounds where the spin-orbit interaction plays an important role.

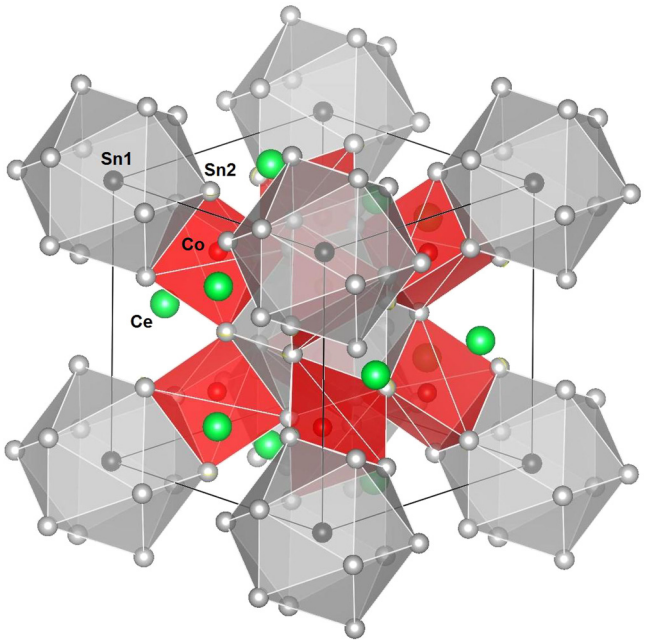

FIG. 1. (Color online) The unit-cell structure of $Ce_3Co_4Sn_{13}$ highlighting the arrangement of the $Sn1(Sn)_{12}$ cages and corner-sharing $Co(Sn2)_6$ trigonal prisms. Ce atoms are shown as green balls, Co atoms are red balls, Sn2 are gray, and Sn1 are dark green balls.

III. RESULTS AND DISCUSSION

A. Covalent bonding in $Ce_3Co_4Sn_{13}$: A reference to covalent bonding in $Ce_3Rh_4Sn_{13}$ and $Ce_3Ru_4Sn_{13}$

Recently [16,17] we presented the electronic structure of La-doped $Ce_3Rh_4Sn_{13}$ and $Ce_3Ru_4Sn_{13}$ and found covalent bonding between atoms in the unit cell. The charge density difference analysis displayed in both compounds a charge accumulation between the d electron type metal M (Rh or Ru) and Sn2 atoms, which implies a strong covalent bonding interaction. The second type of charge accumulation was calculated between the Sn2 atoms with possible contribution from the neighboring Ce and Sn1 atoms. We suggested that these bonding features among metal M and Sn2 atoms as well as between Sn1 and Sn2 could be a reason of slight deformation of $Sn1(Sn)_{12}$ and $Ce(Sn)_{12}$ cages, which indeed is observed at about 160 K [15]. This subtle structural change from the cubic phase to the superlattice variant was observed within the $Ce_3M_4Sn_{13}$ series with accompanying anomalies in electrical resistivity, magnetic susceptibility, and specific heat [13,15]. However, the comparison of the three-dimensional charge density map recently calculated for $Ce_3Rh_4Sn_{13}$ [16] and $Ce_3Ru_4Sn_{13}$ [17] explicitly shows significant difference in $\Delta\rho_e$ inside the trigonal prisms. The charge density $\Delta\rho_e$ is defined as a difference between the electron density of the $Ce_3M_4Sn_{13}$ and the electron density of respective $La_3M_4Sn_{13}$ counterparts to highlight the role of Ce atoms in the binding. Here, we present the charge density analysis for $Ce_3Co_4Sn_{13}$ in order to compare the charge density map calculated for the series of $Ce_3M_4Sn_{13}$ compounds. In result, we hope to explain the various behaviors of the electrical resistivity under pressure, experimentally documented for the corresponding $Ce_3M_4Sn_{13}$ compounds.

Figures 2–4 display the difference in charge density $\Delta\rho_e$, to compare the reorganization of charge distribution between atoms of the $Ce_3M_4Sn_{13}$ compounds. Thus, charge accumulation between Co and Sn2 atoms, shown in Fig. 2, displays a high charge density $\Delta\rho_e$ located in the plane $(00\frac{1}{4})$ between Co and Sn2 atoms, which looks similar to $\Delta\rho_e$ between Rh and Sn2 atoms in $Ce_3Rh_4Sn_{13}$. The $\Delta\rho_e$ distribution in $Ce_3Ru_4Sn_{13}$ is quite different; it shows the maximum in charge density $\Delta\rho_e$ located near Ru atoms.

The change in charge density $\Delta\rho_e$ along the bonding line Sn1−M−Sn1 is for the series of $Ce_3M_4Sn_{13}$ compounds compared in Fig. 3. It is worth noting that the $\Delta\rho_e$ change on Ru is positive, while for $Ce_3Rh_4Sn_{13}$ and $Ce_3Co_4Sn_{13}$ $\Delta\rho_e$ on metal M it is negative. The negative value of $\Delta\rho_e$ indicates the shift of the charge from the Rh and Co atom to inside the $(Sn2)_6$ cage. Figure 4 exhibits $\Delta\rho_e$ change along the line

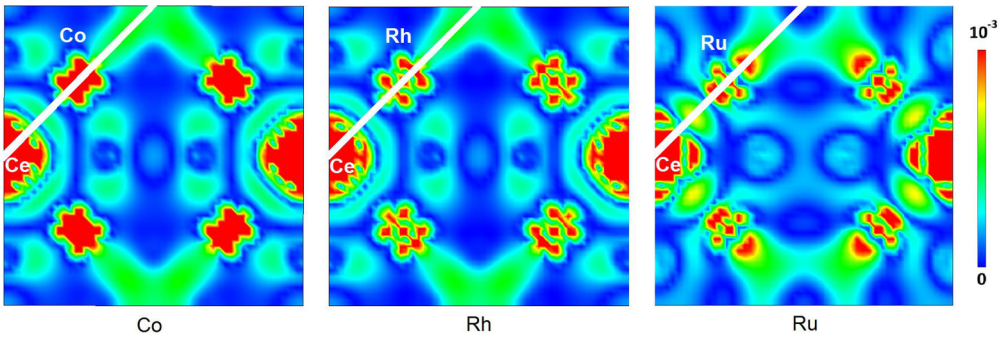

FIG. 2. (Color online) Difference charge density map $\Delta\rho_e$ in electron/Å^3 for $Ce_3Co_4Sn_{13}$ is compared with $\Delta\rho_e$ obtained recently for $Ce_3Rh_4Sn_{13}$ [16] and for $Ce_3Ru_4Sn_{13}$ [17], and comparison of $\Delta\rho_e$ in the plane $(00\frac{1}{4})$. The white dotted line sets the direction of the charge distribution between the metal M and Sn2 atoms located in the plane.

between the atoms Sn1 and Sn2. It seems interesting that the charge accumulation inside the cage $Sn1(Sn2)_{12}$ between Sn1 and Sn2 atoms is for $Ce_3Co_4Sn_{13}$ qualitatively similar to that found for $Ce_3Rh_4Sn_{13}$, but is quite different for $Ce_3Ru_4Sn_{13}$.

B. Band-structure calculations under pressure

The calculated density of states were recently presented for $Ce_3Co_4Sn_{13}$ [21], $Ce_3Rh_4Sn_{13}$ [22], and $Ce_3Ru_4Sn_{13}$ [23]. Here we are more concentrated on the effect of pressure on the band structure of these compounds. To obtain the pressure dependencies of the bands, the respective DOSs were calculated for the hypothetical lattice parameters of $Ce_3Co_4Sn_{13}$ and $Ce_3Ru_4Sn_{13}$ smaller with respect to that measured at room temperature (unit-cell volume decreases with pressure). We used the Birch-Murnaghan isothermal equation of state [24] to estimate hypothetical applied pressure corresponding to systematic decreasing of the unit-cell volume: $V(P) = V(0)[1 + \frac{B'}{B}P]^{-1/B'}$, where $V(0)$ is the unit-cell volume experimentally obtained at room temperature and ambient pressure, while the bulk modulus B_0 and its pressure derivative B' were calculated for the respective compounds (for $Ce_3Co_4Sn_{13}$ we calculated $B = 100.93$ GPa and $B' = 4.82$; for $Ce_3Ru_4Sn_{13}$, $B = 100.65$ GPa and $B' = 4.38$). Figures 5–7 show the pressure dependent DOSs for $Ce_3Co_4Sn_{13}$ and $Ce_3Ru_4Sn_{13}$, respectively. In both cases the metal $M\,d$ bands mainly contribute in the energy range -0.5 to -3 eV, while the $4f$ states form a sharp DOS peak located above the Fermi level in the electronic bands. The small occupation of Ce $4f$ states forms a small peak located at about 0.1 eV below ϵ_F. The electronic structures of the $Ce_3M_4Sn_{13}$ compounds were recently discussed in detail [15,21,22]; here we investigate the change in density of states at high pressure in order to explain opposite trends experimentally observed in the response of $Ce_3Co_4Sn_{13}$ and $Ce_3Ru_4Sn_{13}$ to the applied pressure.

The calculations show the following consequences.

(i) Although the pressure effect on the shape of DOSs either in $Ce_3Co_4Sn_{13}$ or $Ce_3Ru_4Sn_{13}$ is rather small, the density of the electronic states located near the Fermi level with binding energies $|\epsilon - \epsilon_F| \approx k_B T_D$ is evidently pressure dependent. Moreover, the energy shift near ϵ_F for the bands in $Ce_3Co_4Sn_{13}$ is found to be different than that calculated for $Ce_3Ru_4Sn_{13}$. In $Ce_3Ru_4Sn_{13}$ [see Fig. 5(b)] the maximum in total density of states does not show any significant pressure effect (shift) at $\epsilon = \epsilon_F$, while for the energies $|\epsilon - \epsilon_F| \gtrsim 0.1$ eV the DOS simultaneously shifts with increasing pressure towards higher energies $|\epsilon|$ either in the occupied or empty side. In this case

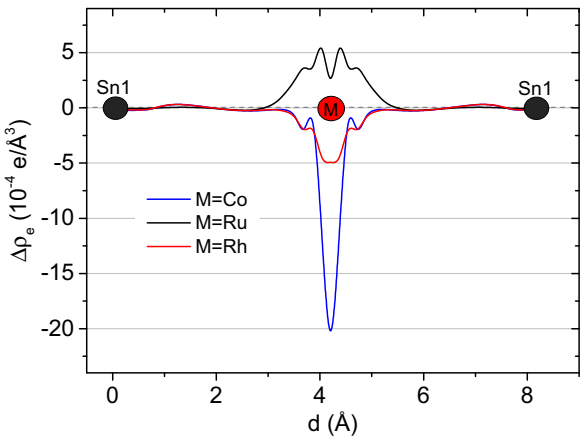

FIG. 3. (Color online) A comparison of the calculated charge density $\Delta\rho_e$ plotted along line representing the nearest-neighbor Sn1−M−Sn1 bonding in the series $Ce_3M_4Sn_{13}$, where M = Co, Rh (the $\Delta\rho_e$ data from Ref. [16]), Ru (cf. Ref. [17]).

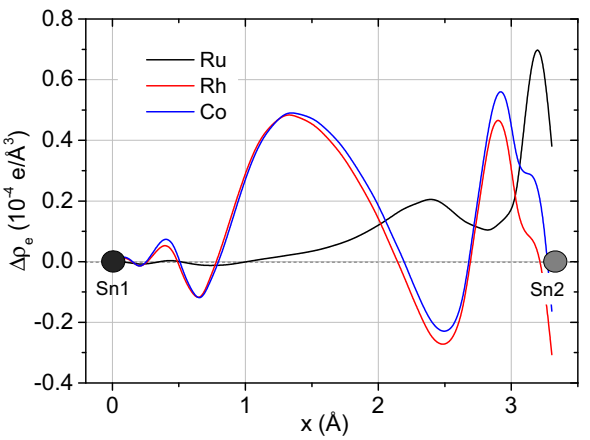

FIG. 4. (Color online) Calculated charge density $\Delta\rho_e$ plotted on the line between Sn1 and Sn2 atoms (cf. Fig. 1) for different $Ce_3M_4Sn_{13}$ compounds, where M = Co, Rh [16], Ru [17].

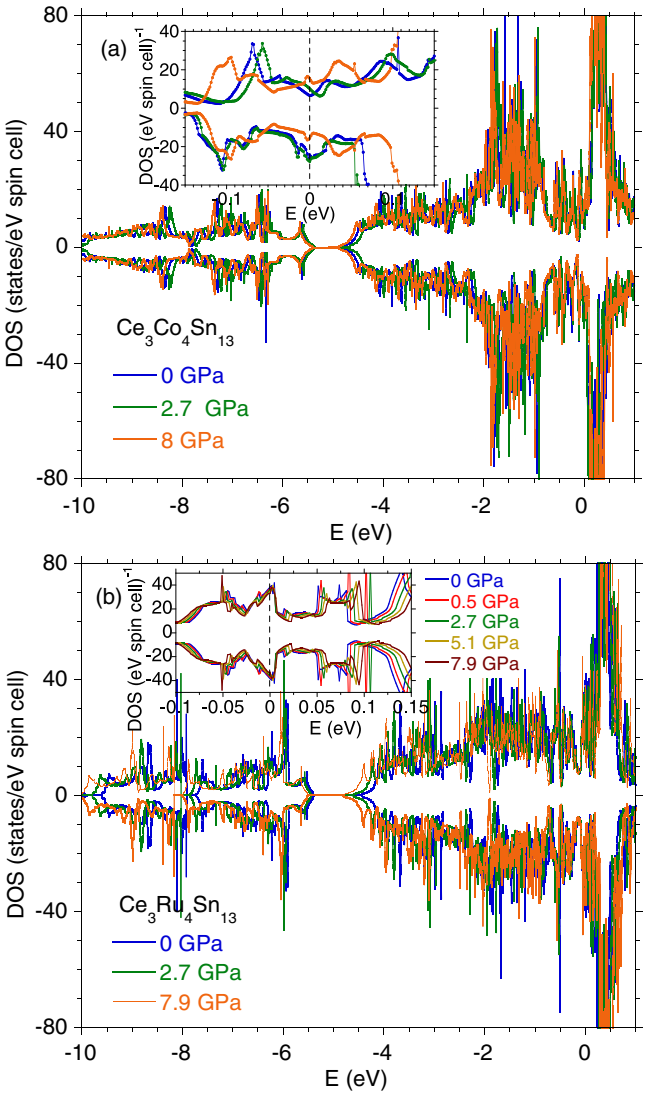

FIG. 5. (Color online) The total and spin-resolved density of states within LSDA approximation at different pressure calculated for $Ce_3Co_4Sn_{13}$ (a) and for $Ce_3Ru_4Sn_{13}$ (b). The inset to panel (a) and (b) displays the details in pressure dependent total DOS near the Fermi energy for the respective compounds. The total DOSs show different energy shifts near ϵ_F for the bands calculated for $Ce_3Co_4Sn_{13}$ (a) and for $Ce_3Ru_4Sn_{13}$ (b); the effect is discussed in Sec. III B.

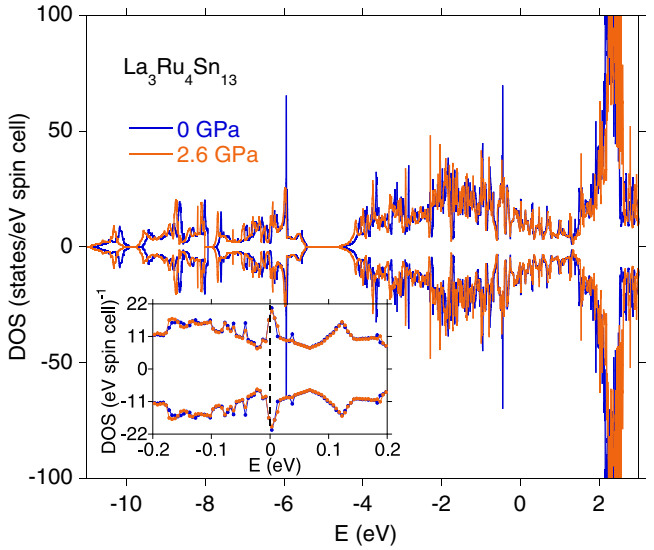

FIG. 6. (Color online) The total and spin-resolved density of states within LSDA approximation under the pressure 0 and 2.6 GPa, calculated for $La_3Ru_4Sn_{13}$. The inset displays the details in pressure dependent total DOS near the Fermi energy. The sharp maximum in DOS at ϵ_F can cause spin waves experimentally observed in $La_3Ru_4Sn_{13}$ (discussion in Sec. III B).

the total DOS at ϵ_F slightly decreases with increasing pressure as shown in the inset to Fig. 5(b). Such variation in DOS with pressure is theoretically predicted for electron-type HF metals [25]. Figure 6 shows a similar sharp peak in the d bands of $La_3Ru_4Sn_{13}$, however the density of states in the vicinity of the Fermi level does not exhibit any pressure dependence, characteristic of $Ce_3Ru_4Sn_{13}$. For $Ce_3Co_4Sn_{13}$ the pressure effect on the bands near the Fermi energy is, however, different [see the inset to Fig. 5(a)]. Here, the total DOS exhibits for $P = 0$ the pseudo-gap-like interband distance, which separates two pronounced maxima of the f electron states hybridized with the conduction electron states, located symmetrically at about 0.07–0.09 eV below and above ϵ_F. Both maxima first move towards ϵ_F with P in the range of $P < 2.7$ GPa (this means that the f DOSs are located at lower energy $|\epsilon|$ in the occupied and empty bands for $P < 2.7$). This pressure behavior is characteristic of hole-type HF metals [25], while the opposite trend is observed for $P > 2.7$ GPa, suggesting the electron-type conductivity at higher pressure.

(ii) Both $Ce_3Ru_4Sn_{13}$ and $La_3Ru_4Sn_{13}$ compounds exhibit a sharp peak in the total DOS located exactly at the Fermi energy [see Figs. 5(b) and 6], which mainly represents the Ru $4d$ electron states and also the amount of Ce $4f$ and $5d$ electron states in $Ce_3Ru_4Sn_{13}$ or Ru $4d$ electron states in $La_3Ru_4Sn_{13}$, which are strongly hybridized with the band states, respectively. There is probably the same origin of negative $d\rho/dP$ pressure effect in these two compounds, regardless of whether magnetic Ce or nonmagnetic La is involved. The high DOS at ϵ_F increases the electron-phonon interaction, therefore one possible explanation is that electron-phonon coupling drives the observed negative pressure dependencies in $Ce_3Ru_4Sn_{13}$ and $La_3Ru_4Sn_{13}$. This scenario, however, is questionable taking into account a whole series of $Ce_3M_4Sn_{13}$ and $La_3M_4Sn_{13}$ isostructural compounds with very similar phonon spectra and enhanced value of DOS at ϵ_F, which is for $Ce_3Co_4Sn_{13}$ and $Ce_3Rh_4Sn_{13}$ about $1/2$ of $N(\epsilon_F)$ obtained for $Ce_3Ru_4Sn_{13}$. Another scenario assumes that high $N(\epsilon_F)$ not only increases the electron-phonon interaction but also strengthens the spin fluctuations. For $Ce_3Ru_4Sn_{13}$ and $La_3Ru_4Sn_{13}$ a sharp peak of $4d$ electron states at ϵ_F indeed could lead to d electron spin fluctuations (e.g., in similar cage $CeRhSn_2$ and $LaRhSn_2$ [26] or $CeRh_2Sn_4$ and $LaRh_2Sn_4$ [27] a Fermi-surface analysis shows that there are some parallel sections of the d electron sheets which could generate nesting instabilities and be responsible for the spin fluctuation effects), which seem to be important to explain experimentally observed P dependence in resistivity for $Ce_3Ru_4Sn_{13}$ and $La_3Ru_4Sn_{13}$. Moreover, the resistivity of $La_3Ru_4Sn_{13}$ is well approximated by the $T^{5/3}$ law from 8 K ($La_3Ru_4Sn_{13}$ shows

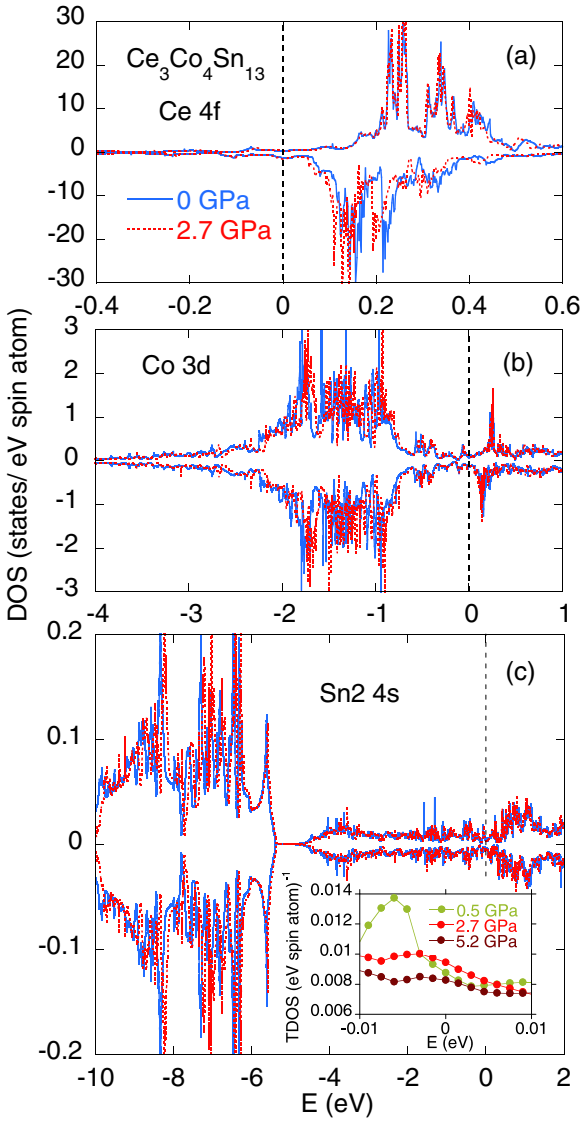

FIG. 7. (Color online) Atomic partial $4f$ density of states for Ce (a), $3d$ states for Co (b), and Sn2 $4s$ states (c) obtained for $Ce_3Co_4Sn_{13}$ at different pressure; the figure compares the data obtained for $P = 0$ and 2.7 GPa. The inset displays Sn2 $4s$ conduction states for energies $|\epsilon - \epsilon_F| \approx k_B T_D$.

a superconducting state below ∼4 K [38]) up to ∼40 K at the applied hydrostatic pressures, demonstrating the persistence of the contribution of spin fluctuations to the resistivity.

(iii) In Table I we summarize the density of states at the Fermi energy for both compounds. The $N(\epsilon_F)$ explicitly decreases with increasing P. In the table also are listed the energies ϵ_f of the maxima in Ce $4f$ states with respect to the Fermi level [28]. In effect, the high-temperature logarithmic slope in resistivity above the Kondo temperature and the high-temperature ρ value vary with P, which may indicate that $|J_{fs}^3 N(\epsilon_F)|$ in the Kondo lattice system [29] varies with P too. Regarding the coupling constant J_{fs}, we consider the Schrieffer-Wolf expression $J_{fs} = \frac{2V_{fs}^2}{|\epsilon_f - \epsilon_F|}$ [30], where $V_{fs} = [\Delta/\pi N(\epsilon_F)]^{1/2}$ is the f conduction-band hybridization matrix element. The hybridization parameter

TABLE I. The pressure dependencies of total density of states $N(\epsilon_F)$, hybridization matrix element V_{fs}, energy of the maxima of f electron states in relation to the Fermi level, and J_{fs} interaction between the f electron states and the conduction-band states for $Ce_3Co_4Sn_{13}$ and $Ce_3Ru_4Sn_{13}$.

Compound	P (GPa)	$N(\epsilon_F)$ (eV^{-1} f.u.$^{-1}$)	V_{fs} (meV)	$\lvert\epsilon_f - \epsilon_F\rvert$ (eV)	J_{fs} (meV)
$Ce_3Co_4Sn_{13}$	0	15.7	53.4	0.09	65.7
	0.5	14.9	54.7	0.09	65.6
	2.7	18.8	49.2	0.08	60.4
	5.2	16.7	51.7	0.085	59.4
	8.0	15.5	53.6	0.09	60.5
	11.2	15.4	53.8	0.09	64.3
	14.8	14.0	56.3	0.095	66.1
	18.9	11.5	62.2	0.11	70.4
	23.6	10.4	65.5	0.11	77.9
$Ce_3Ru_4Sn_{13}$	0	38.3	24.1	0.043	26.9
	0.5	37.5	24.7	0.045	27.0
	2.7	35.8	24.9	0.046	27.0
	5.1	35.0	25.2	0.047	27.1
	7.9	33.2	25.9	0.05	27.0
	10.9	34.4	25.5	0.053	24.9
	14.4	32.2	26.3	0.055	25.2
	18.3	30.0	27.3	0.058	25.6
	22.7	27.8	28.3	0.063	25.4

Δ which describes the hybridization part of the Anderson impurity Hamiltonian [31] was recently obtained from the core level Ce $3d$ x-ray photoemission spectroscopy (XPS) spectra [15] using the Gunnarsson and Schönhammer method; for details see Refs. [32–34]. The applied pressure increases hybridization V_{fs} and in consequence increases J_{fs}; see Fig. 8.

As shown in Table I pressure explicitly changes the hybridization matrix element V_{fs}. Previous experiments [35] confirmed that the pressure tends to promote an increase in hybridization for the electron-type heavy-fermion metals, while the pressure leads to the opposite effect for the hole-type

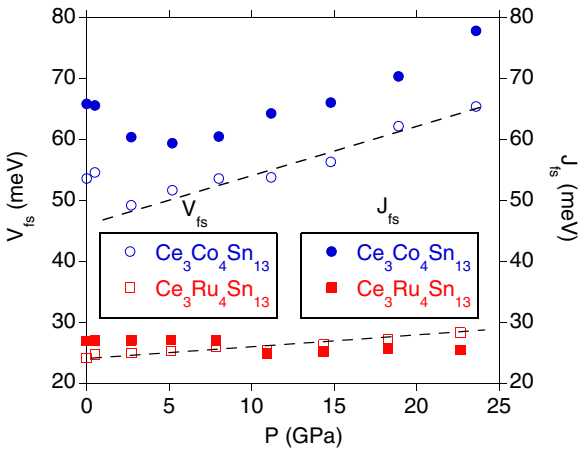

FIG. 8. (Color online) The pressure dependence of the hybridization matrix element $V_{fs} = [\Delta/\pi N(\epsilon_F)]^{1/2}$, where $\Delta \approx 140$ meV for $Ce_3Co_4Sn_{13}$ and ∼70 meV for $Ce_3Ru_4Sn_{13}$ (cf. Ref. [15]), and J_{fs} coupling between f electron and conduction-band states vs P.

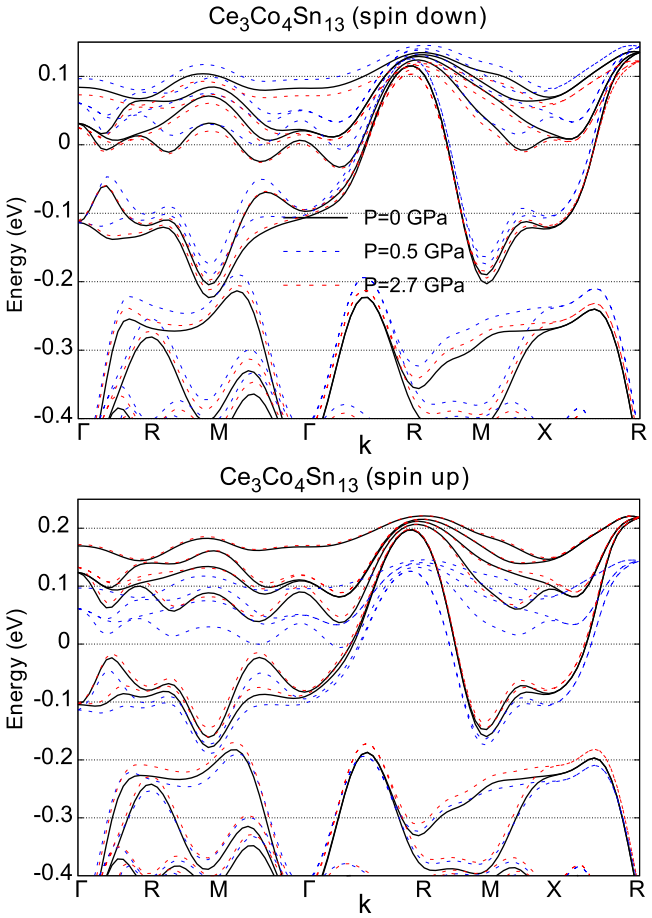

FIG. 9. (Color online) The energy-band structure of $Ce_3Co_4Sn_{13}$ for spin-up and spin-down channels along the high symmetry directions.

HF compounds. We therefore suggest that the decrease of V_{fs} and J_{fs} obtained with increasing P for $Ce_3Co_4Sn_{13}$ within $P < \sim 3$ GPa can among other things correspond to a hole-type character of this compound.

(iv) The dispersion curves calculated for applied pressure along the Γ-R-M-Γ-R-M-X-M k path in the reciprocal primitive cell are shown in Figs. 9 and 10 for $Ce_3Co_4Sn_{13}$ and $Ce_3Ru_4Sn_{13}$, respectively. In the case of $Ce_3Ru_4Sn_{13}$, the character of the spin-up and spin-down states in the vicinity of ϵ_F remains the same, while the energy-band structure of $Ce_3Co_4Sn_{13}$ for spin-up and spin-down channels is slightly different. Moreover, the spin polarized bands calculated for $Ce_3Co_4Sn_{13}$ show an interband distance of majority-spin band structure at ϵ_F in Γ-R-M, Γ-M, and X-M k directions which is, however, not visible in the band structure of $Ce_3Ru_4Sn_{13}$. The similar interband distance of minority-spin band structure in $Ce_3Co_4Sn_{13}$ is clearly observed in Fig. 9 (upper panel) for $P \neq 0$. This interband distance versus P change correlates with the electrical resistivity data under external pressure, as shown in Fig. 11(a), which means that the semimetallic character of $Ce_3Co_4Sn_{13}$ is stabilized by pressure and explains the strong and positive $\frac{d\rho}{dP}$ effect in the temperature range $T < T_D$.

One can also assume a small concentration δ of vacancies in the 2a sites (see Ref. [22]) as another reason for semimetallic

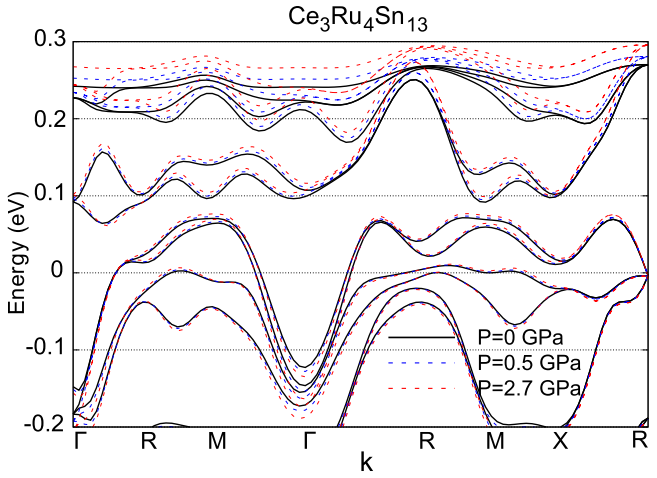

FIG. 10. (Color online) The energy-band structure of $Ce_3Ru_4Sn_{13}$ for the spin-up channel. The band structure for spin-up and spin-down channels is the same.

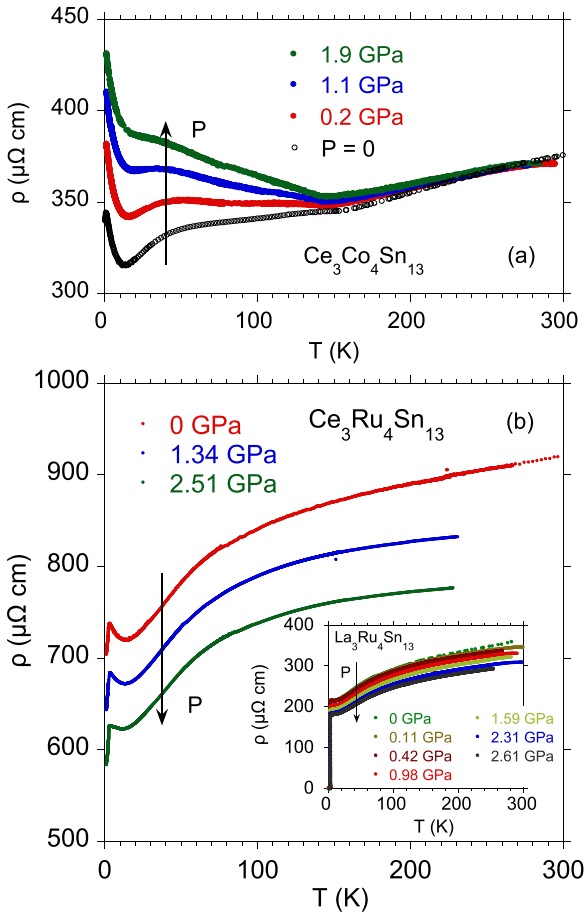

FIG. 11. (Color online) Electrical resistivity for $Ce_3Co_4Sn_{13}$ (a) (these ρ vs P data were previously presented in Ref. [12]) and $Ce_3Ru_4Sn_{13}$ (b) under applied pressure. The inset to panel (b) displays the resistivity of $La_3Ru_4Sn_{13}$ vs pressure (cf. Ref. [38]). For $Ce_3Co_4Sn_{13}$ and $Ce_3Rh_4Sn_{13}$ (cf. Ref. [12]) the effect is observed rather weakly above T_D (where T_D is the temperature of the crystallographic distortion), while at the low-temperature range the effect is significant.

character of the off-stoichiometric $Ce_3Co_4Sn_{13-\delta}$. As a result of the inclusion of vacancies, another *pseudo-gap*-like interband distance shown in Fig. 9 at about −0.2 eV in the bands of the stoichiometric compound can move towards Fermi level, which in consequence could also give the pressure increase of ρ. The effect of subtle changes of the bands in the vicinity of the Fermi level is hypothetically possible. To prove it, we calculated the band structure for $Ce_3Co_4Sn_{13-\delta}$ simulating the vacancies in the $2a$ sites by considering a Sn number of electrons Z slightly lower than 50. This procedure indeed shifts the −0.2 eV pseudogap to the Fermi level for $Z = 49.9$, which is equivalent of $\delta = 0.65$ (the results are not shown here). Although such a large number of vacancies has not been demonstrated by microanalysis [11], the semimetallic character of $Ce_3Co_4Sn_{13}$ resulting from Sn vacancies seems to be possible.

In the both Ce-based systems the bands form the holelike Fermi surface along Γ-R-M, Γ-M, and X-M directions, which can also contribute to pressure dependencies of the low-temperature resistivity in these heavy-fermion compounds.

Here, we have presented calculations for several compounds with $Ce_3M_4Sn_{13}$ stoichiometry. In order to compare different compounds in a consistent way, we decided to carry out our calculations without additional $4f$ correlations, namely, for $U = 0$. There is no reason why in case of LSDA + U calculations the U parameter should be for all compounds the same. The usual way to determine U is to compare the experimental XPS spectra with calculations for different U values. However, in our case the $4f$ contribution to XPS measurement is masked by the d states of the transition elements. Moreover, the minimal spin polarization observed from magnetization data also suggests a very small value of U across the investigated compounds, as even moderate U usually gives substantial moments located on Ce atoms due to splitting of Ce $4f$ states [36]. It should be also noted that LSDA + U calculations can lead to various ground states depending on initial density matrix setup. The initial conditions can change the obtained ground state. Therefore, one should also choose the initial conditions in such a way that the obtained ground state will match the experimental data or at least be weakly dependent on initial conditions. Finally, U can be included in calculations in several ways [37]; in a real system the additional correlations should be some weighted average between the fully localized limit and around the mean field approach. Here, the weight would also have to be different for different M elements in $Ce_3M_4Sn_{13}$, which would make comparison of subtle DOS features impossible. For several $Ce_3M_4Sn_{13}$ compounds there are just too many free parameters within LSDA + U to make reasonable and consistent predictions about the subtle shape of DOS near Fermi level.

IV. ELECTRICAL RESISTIVITY OF THE HEAVY-FERMION-FILLED CAGE COMPOUND $Ce_3M_4Sn_{13}$ (M = Co, Rh, Ru) AT HIGH PRESSURE, CONCLUDING REMARKS

Figure 11 displays electrical resistivity for $Ce_3Co_4Sn_{13}$ (a) and $Ce_3Ru_4Sn_{13}$ (b) under applied pressure. In panel (a) the pressure effect is strong and positive below the temperature $T_D \approx 160$ K, where the subtle structural transition due to deformation of the $(Sn2)_{12}$ cages was reported [15]. Our band-structure calculations indicate for a ground state ($T = 0$) of $Ce_3Co_4Sn_{13}$ a semimetallic character, which is enhanced in applied pressure; cf. Fig. 9(b). For simplicity in *ab initio* calculations we did not take into account the low-temperature superlattice variant of the cubic structure, however we have found strong charge accumulation between Co and Sn2 atoms, which can be a reason of strong covalent bonding and as a result of structural distortion below T_D. Due to the fact that the positive value of $\frac{d\rho}{dP}$ is clearly visible either for $Ce_3Co_4Sn_{13}$ [cf. Fig. 11(a)] or $Ce_3Rh_4Sn_{13}$ [12] for $T < T_D$, we limit our discussion only to the low-temperature region (i.e., for $T < T_D$), although the pressure effect is pronounced over the range of T for Ru samples, and signals quite different nature. The interband distance at $\sim\epsilon_F$ is stable at high pressure, while the number of conduction $4s$ Sn2 electrons evidently decreases within energies $|\epsilon - \epsilon_F|/k_B < 160$ K; both effects explain the positive value of $\frac{d\rho}{dP} > 0$ below T_D. For $T > T_D$ the increase of ρ with pressure is observed to be much smaller and can be explained by a change of T_{coh} with P, characteristic of the heavy fermion. The holelike bands at the Fermi energy are in $Ce_3Co_4Sn_{13}$ another reason for the increase of $\frac{d\rho}{dP}$ with pressure. It has been documented theoretically [25] for the hole-type HF metals that the electrical resistivity ρ increases with pressure below $T = T_{max}$, in case of $Ce_3Co_4Sn_{13}$ $T_{max} \equiv T_{coh} \sim 60$ K [11], and the holelike pressure effect giving additional contribution to the resistivity is possible. Figure 12 exhibits $\frac{d\rho}{dP}$ for the series of $Ce_3M_4Sn_{13}$ and respective La counterparts [the P-dependent $\rho(T)$ data are presented in Ref. [38]]. The $\frac{d\rho}{dP} > 0$ behavior under pressure, experimentally documented for $La_3Co_4Sn_{13}$ [39], can be interpreted as a result of its band-structure properties

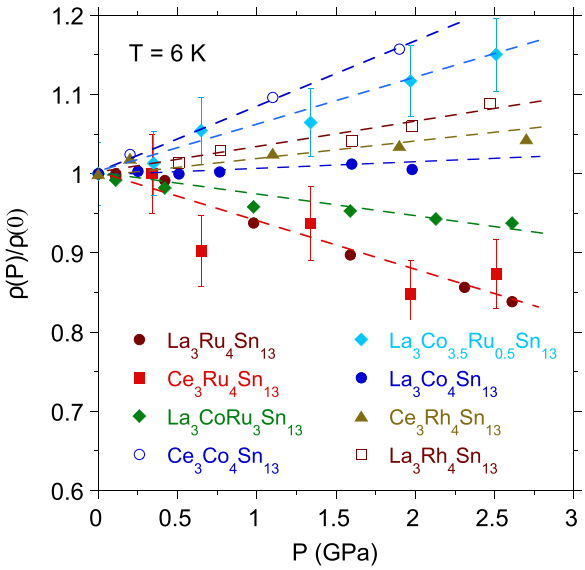

FIG. 12. (Color online) Electrical resistivity ρ at $T = 6$ K vs pressure, normalized to ρ at $T = 6$ K and $P = 0$ for the series of $Ce_3M_4Sn_{13}$ and the La counterparts. The $\rho(T)$ vs P data were taken for $Ce_3Rh_4Sn_{13}$ from Ref. [12], while for respective La-reference compounds from Refs. [38,39].

near the Fermi energy similar to that in $Ce_3Co_4Sn_{13}$, and the holelike scattering process [21].

Within the series of $Ce_3M_4Sn_{13}$, a similar positive $\frac{d\rho}{dP}$ effect is explicitly shown for $Ce_3Co_4Sn_{13}$ and $Ce_3Rh_4Sn_{13}$ in the temperature region $T < T_D$ (cf. Fig. 12 and Ref. [12]), which suggests a similar complex mechanism for ρ versus P behavior in the $Ce_3Rh_4Sn_{13}$ and $Ce_3Co_4Sn_{13}$ compounds. Indeed, the electrical resistivity of $Ce_3Rh_4Sn_{13}$ increases with pressure for $T < T_D$ [12] and the charge accumulation between Rh and Sn2 atoms shown in Fig. 2 is very similar to that calculated for $Ce_3Co_4Sn_{13}$. If we assume that the local distortion of Sn cages can be a reason of changes in the energetic bands near the Fermi energy, and consequently affects the ρ versus P, then quite different charge distribution between Ru and Sn2 atoms shown in Figs. 2 and 4 explains the rather weak distortion effect observed in $Ce_3Ru_4Sn_{13}$, and its impact on $\frac{d\rho}{dP}$. Therefore, the negative electrical resistivity variation with pressure shown in Fig. 12 for $Ce_3Ru_4Sn_{13}$ can be discussed as a result of the pressure variation of DOS at ϵ_F. However, since the negative ρ versus P change for $Ce_3Ru_4Sn_{13}$ below the temperature $T_{\text{inf}} \sim 50$ K of the inflection in $\rho(T)$ can be explained theoretically for the electron-type HF Ce-based metal [25], the decrease in ρ with P for temperatures $T > T_{\text{inf}}$ is in contrast to theoretical predictions. Even more difficult to explain is the observed decrease of resistivity ρ with P in a wide temperature range for the $La_3Ru_4Sn_{13}$ counterpart, as shown in the inset to Fig. 11. The *negative* effect of pressure is, however, expected for the spin fluctuated system as a result of the increased delocalization of f or d states due to hybridization with the conduction electron states. In fact, almost all the high-pressure studies on spin-fluctuation systems reported so far indicate suppression of spin fluctuation under pressure and in consequence the decrease of the resistivity with P [40–42]. This can be the case for $Ce_3Ru_4Sn_{13}$ and its La counterpart. Very recently [23] we presented the total energy of the simulated $Ce_3Ru_4Sn_{13}$ crystal versus fixed spin moment (FSM) derived from FSM calculations using the virtual crystal approximation. The calculations showed a broad minimum at about 4 μ_B per unit cell which suggests that the compound becomes magnetically unstable. We also calculated total energy versus FSM for $Ce_3Co_4Sn_{13}$, which did not exhibit any minimum and confirmed that the Co system forms a more stable nonmagnetic ground state. From the above discussion it appears that the magnetic instability of $Ce_3Ru_4Sn_{13}$ and $La_3Ru_4Sn_{13}$ can qualitatively explain the high-pressure ρ effect in any temperature range.

V. CONCLUDING REMARKS

The contrasting pressure dependent effects in resistivity of $Ce_3Co_4Sn_{13}$ and $Ce_3Ru_4Sn_{13}$ heavy-fermion compounds are discussed as revealing the different band-structure properties of these systems under pressure. In a heavy-fermion system the increase of the resistivity with pressure, reported above the characteristic temperature T_K or T_{max}, is ascribed to the increase of J_{fs} coupling between f electron and conduction electron states with pressure. This can be one of the possible reasons for the positive value of $\frac{d\rho}{dP}$ in $Ce_3Co_4Sn_{13}$ and $Ce_3Rh_4Sn_{13}$, however a similar positive $\frac{d\rho}{dP}$ behavior is also documented for respective La references. The effects of pressure on $Ce_3Co_4Sn_{13}$ and $La_3Co_4Sn_{13}$ are studied in the framework of FPLO band-structure calculations. We documented that the main cause of $\frac{d\rho}{dP} > 0$ behavior is the interband distance located at the Fermi level in the energy bands. This interband distance *increases* with pressure and leads to strong increase in ρ under pressure; the effect is especially strong for $T < T_D$. In case of $Ce_3Ru_4Sn_{13}$ and $La_3Ru_4Sn_{13}$ the resistivity decreases with pressure; this opposite and unusual for HF materials pressure effect is attributed to the suppression of spin fluctuation under pressure. Finally, we noted that the charge density distribution between metal M and Sn2 atoms in the system of $Ce_3M_4Sn_{13}$ compounds is very similar for $M =$ Co and Rh, while quite different for $M =$ Ru. The different covalent bondings, resulting from the charge density distribution in the plane $(00\frac{1}{4})$, lead to local structural distortion of the cages in $Ce_3Co_4Sn_{13}$ and $Ce_3Rh_4Sn_{13}$, and in consequence to semimetallic properties below the temperature of structural distortion T_D.

ACKNOWLEDGMENTS

Research was supported by National Science Centre on the basis of Decision No. DEC-2012/07/B/ST3/03027. The authors would like to thank Prof. M. B. Maple from University of California at San Diego for scientific cooperation, especially for the opportunity to perform measurements at high pressure.

[1] S. Doniach, Physica B **91**, 231 (1977).
[2] S. Yomo, L. Gao, R. L. Meng, P. H. Hor, C. W. Chu, and J. Susaki, J. Magn. Magn. Mater. **76–77**, 257 (1988).
[3] Y.-Y. Chen, J. M. Lawrence, J. D. Thompson, and J. O. Willis, Phys. Rev. B **40**, 10766 (1989).
[4] B. Bellarbi, A. Benoit, D. Jaccard, J. M. Mignot, and H. F. Braun, Phys. Rev. B **30**, 1182 (1984).
[5] M. C. Aronson, J. D. Thompson, J. L. Smith, Z. Fisk, and M. W. McElfresh, Phys. Rev. Lett. **63**, 2311 (1989).
[6] H. D. Yang and W. H. Lee, Phys. Rev. B **43**, 3664 (1991).
[7] Y. Itoch, H. Kadomatsu, M. Kurisu, and H. Fujiwara, J. Phys. Soc. Jpn. **56**, 1159 (1987).
[8] J. D. Thompson and J. M. Lawrence, in *Handbook on the Physics and Chemistry of Rare Earths*, edited by K. A. Gschneidner, Jr. and K. Eyring (North-Holland, 1994), Vol. 19, Chap. 133.
[9] For $Ce_3Co_4Sn_{13}$ the Kondo temperature $T_K \approx 1.5$ K, whereas the quantum coherence appointed by the maximum in $\rho(T)$ data is not clearly visible, therefore the increase of the electrical resistivity under pressure in respect to the $\rho(T)$ data at $P = 0$ could be observed in the wide temperature range for $T > T_K$.
[10] A. L. Cornelius, A. D. Christianson, J. L. Lawrence, V. Fritsch, E. D. Bauer, J. L. Sarrao, J. D. Thompson, and P. G. Pagliuso, Physica B **378–380**, 113 (2006).

[11] A. Ślebarski, M. Fijałkowski, and J. Goraus, Intermetallics **54**, 199 (2014).
[12] A. Ślebarski, B. D. White, M. Fijałkowski, J. Goraus, J. J. Hamlin, and M. B. Maple, Phys. Rev. B **86**, 205113 (2012).
[13] E. L. Thomas, H.-O. Lee, A. N. Bonkston, S. MaQuilon, P. Klavins, M. Moldovan, D. P. Young, Z. Fisk, and J. Y. Chan, J. Solid State Chem. **179**, 1642 (2006).
[14] C. S. Lue, H. F. Liu, S.-L. Hsu, M. W. Chu, H. Y. Liao, and Y. K. Kuo, Phys. Rev. B **85**, 205120 (2012).
[15] A. Ślebarski and J. Goraus, Phys. Rev. B **88**, 155122 (2013).
[16] A. Ślebarski, P. Witas, J. Goraus, L. Kalinowski, and M. Fijałkowski, Phys. Rev. B **90**, 075123 (2014).
[17] A. Ślebarski, J. Goraus, P. Witas, L. Kalinowski, and M. Fijałkowski, Phys. Rev. B **91**, 035101 (2015).
[18] J. P. Remeika, G. P. Espinosa, A. S. Cooper, H. Barz, J. M. Rowel, D. B. McWhan, J. M. Vandenberg, D. E. Moncton, Z. Fizk, L. D. Woolf, H. C. Hamaker, M. B. Maple, G. Shirane, and W. Thomlinson, Sol. State Commun. **34**, 923 (1980); J. L. Hodeau, M. Marezio, J. P. Remeika, and C. H. Chen, *ibid.* **42**, 97 (1982).
[19] K. Koepernik and H. Eschrig, Phys. Rev. B **59**, 1743 (1999); I. Opahle, K. Koepernik, and H. Eschrig, *ibid.* **60**, 14035 (1999); K. Koepernik, B. Velicky, R. Hayn, and H. Eschrig, *ibid.* **55**, 5717 (1997); H. Eschrig, K. Koepernik, and I. Chaplygin, J. Solid State Chem. **176**, 482 (2003); www.fplo.de.
[20] J. P. Perdew and Y. Wang, Phys. Rev. B **45**, 13244 (1992).
[21] G. Zhong, X. Lei, and J. Mao, Phys. Rev. B **79**, 094424 (2009).
[22] M. Gamża, W. Schnelle, A. Ślebarski, U. Burkhardt, R. Gumeniuk, and H. Rosner, J. Phys.: Condens. Matter **20**, 395208 (2008).
[23] A. Ślebarski, M. Fijałkowski, J. Goraus, L. Kalinowski, and P. Witas, J. Alloys Compds. **615**, 921 (2014).
[24] F. D. Murnagham, Proc. Natl. Acad. Sci. USA **30**, 244 (1944); F. Birch, Phys. Rev. **71**, 809 (1947).
[25] L. Hai, L. Zhengzhong, X. Mingwen, and X. Xiaohua, Commun. Theor. Phys. (Beijing, China) **31**, 49 (1999); S. Shang, Phys. Rev. B **65**, 064407 (2002).
[26] M. Gamża, A. Ślebarski, and H. Rosner, J. Phys.: Condens. Matter **20**, 025201 (2008).
[27] M. Gamża, W. Schnelle, R. Gumeniuk, Yu. Prots, A. Ślebarski, H. Rosner, and Yu. Grin, J. Phys.: Condens. Matter **21**, 325601 (2009).
[28] The $4f$ peak is located above the Fermi energy. The increase of the energy $|\epsilon_f - \epsilon_F|$ noted in Table I and accompanying decrease in density of Ce $4f$ correlated states suggest that only the Fermi energy shifts towards lower binding energy. However, within the DFT calculations the Fermi energy is determined by the band structure, as it is calculated by integration of the DOSs up to total number of the valence electrons in the system. Hence, these two quantities: DOS and ϵ_F are related to each other.
[29] B. Cornut and B. Coqblin, Phys. Rev. B **5**, 4541 (1972).
[30] J. R. Schrieffer and P. A. Wolff, Phys. Rev. **149**, 491 (1966).
[31] P. W. Anderson, Phys. Rev. **124**, 41 (1961).
[32] O. Gunnarsson and K. Schönhammer, Phys. Rev. B **28**, 4315 (1983).
[33] J. C. Fuggle, F. U. Hillebrecht, Z. Zolnierek, R. Lässer, Ch. Freiburg, O. Gunnarsson, and K. Schönhammer, Phys. Rev. B **27**, 7330 (1983).
[34] A. Ślebarski, T. Zawada, J. Spałek, and A. Jezierski, Phys. Rev. B **70**, 235112 (2004).
[35] J. D. Thompson, H. A. Borges, Z. Fisk, S. Horn, R. D. Parks, and G. L. Wells, in *Theoretical and Experimental Aspects of Valence Fluctuations and Heavy Fermions*, edited by L. C. Gupta and K. Malik (Plenum, New York, 1987), p. 151.
[36] J. Goraus, A. Ślebarski, and M. Fijałkowski, Intermetallics **32**, 219 (2013).
[37] A. G. Petukhov, I. I. Mazin, L. Chioncel, and A. I. Lichtenstein, Phys. Rev. B **67**, 153106 (2003); M. T. Czyżyk and G. A. Sawatzky, *ibid.* **49**, 14211 (1994); V. I. Anisimov, I. V. Solovyev, M. A. Korotin, M. T. Czyżyk, and G. A. Sawatzky, *ibid.* **48**, 16929 (1993); V. I. Anisimov, J. Zaanen, and O. K. Andersen, *ibid.* **44**, 943 (1991).
[38] A. Ślebarski, M. M. Maśka, M. Fijałkowski, C. A. McElroy, and M. B. Maple, J. Alloys Compds. **646**, 866 (2015).
[39] A. Ślebarski, M. Fijałkowski, M. M. Maśka, M. Mierzejewski, B. D. White, and M. B. Maple, Phys. Rev. B **89**, 125111 (2014).
[40] R. Jullien, M. T. Bèal-Monod, and B. Coqublin, Phys. Rev. B **9**, 1441 (1974).
[41] E. Louis, A. De Visser, A. Menovsky, and J. J. M. Franse, Physica B **144**, 48 (1986), and references therein.
[42] Y. Shimizu, D. Braithwaite, B. Salce, T. Combier, D. Aoki, E. N. Hering, S. M. Ramos, and J. Flouquet, Phys. Rev. B **91**, 125115 (2015).